Universal behavior of electrons & positrons in extensive air showers

S. Lafebre*, R. Engel†, H. Falcke*‡, J. Hörandel*, T. Huege†, J. Kuijpers* and R. Ulrich†

*Department of Astrophysics, IMAPP, Radboud University, P.O. Box 9010, 6500GL Nijmegen, The Netherlands
† Institut für Kernphysik, Forschungszentrum Karlsruhe, P.O. Box 3640, 76021 Karlsruhe, Germany
‡ Radio Observatory, Astron, Dwingeloo, P.O. Box 2, 7990AA Dwingeloo, The Netherlands
§Tyrell Inc., 123 Replicant Street, Los Angeles, California 90210–4321

***Abstract*. Using a large set of CORSIKA simulated extensive air showers at energies 10^{17}–10^{20} eV, we discuss universality features of electron and positron distributions in very-high-energy cosmic-ray air showers. A study of these distributions as a function of particle energy, vertical and horizontal momentum angle, lateral distance, and time distribution of the shower front reveals that most of them depend only on the depth relative to the shower maximum and the number of particles in the cascade at this depth. We empirically derived parameterizations for these distributions, allowing direct access to a realistic description of electron–positron quantities of extensive air showers at very high energy. Data analysis and simulations of electromagnetic effects such as Cherenkov radiation, fluorescence signal, and radio emission can benefit from these parameterizations.**

***Keywords*: Extensive air showers; electron distributions; Shower front structure**

I. INTRODUCTION

Secondary radiation effects in extensive air showers, including atmospheric fluorescence, Cherenkov light and radio signal, primarily depend on the distributions of electrons and positrons in extensive air showers. Here, we investigate dependence of these distributions on energy, species, and zenith angle of the primary particle and on the evolution stage of the shower, extending the concept of universality from previous studies [1, 2, 3, 4, 5].

II. METHOD

Electron and positron distributions in the atmosphere were studied through CORSIKA simulations [6] for protons, photons, and iron nuclei at primary energies of 10^{17}, 10^{18}, 10^{19}, and 10^{20} eV. For each combination of primary particle and energy, showers with zenith angles of 0, 30, 45, and 60° were calculated. Non-vertical showers were injected from different directions to accommodate deviations due to the geomagnetic field. Each parameter set was repeated 20 times, amounting to a total of 3840 simulated showers.

We describe electron and positron distributions in terms of relative evolution stage t, defined in terms of the depth relative to the slant depth $X_{\max}$ where the number of particles in the air shower reaches its maximum:

$$t \equiv \frac{X - X_{\max}}{X_0}, \tag{1}$$

where $X_0 \simeq 36.7$ g/cm^2 is the radiation length of electrons in air. Describing a set of showers in terms of this quantity rather than X or shower age s leads to a higher degree of universality [7, 8].

The total number of particles in the air shower crossing a plane at level t perpendicular to the primary's trajectory is $N(t)$. We define

$$n(t;\mu) \equiv \frac{1}{N(t)}\frac{\partial N(t)}{\partial \mu} \quad \text{and} \tag{2}$$

$$n(t;\mu,\nu) \equiv \frac{1}{N(t)n(t;\mu)}\frac{\partial^2 N(t)}{\partial \mu\, \partial \nu}, \tag{3}$$

as the normalised differential number of particles with respect to some variables μ and ν, with dimension $[\mu]^{-1}$ and $[\nu]^{-1}$, respectively.

III. ENERGY SPECTRUM

From cascade theory, the energy spectrum of electrons and positrons as a function of shower age takes an analytical form as derived by Rossi & Greisen [9]; a thorough previous study of this parameterization was done by Nerling et al. [4]. Loosely translating this description in terms of t, we replace the equation by

$$n(t;\ln\epsilon) = \frac{A_0 \epsilon^{\gamma_1}}{(\epsilon+\epsilon_1)^{\gamma_1}(\epsilon+\epsilon_2)^{\gamma_2}}, \tag{4}$$

where ϵ is the energy of a given secondary particle in the shower, and $\epsilon_{1,2}$ depend on t. We have performed a fit to this function for electrons, positrons and their sum, indirectly providing a description of the negative charge excess of extensive air showers as a function of evolution stage and secondary energy. In these fits the exponent γ_1 was fixed at $\gamma_1 = 2$ for positrons and $\gamma_1 = 1$ for both electrons and the total number of particles. The parameters for all three cases are explained in [8].

When applied to showers initiated by different species at different energies, the energy distribution (4) is reconstructed accurately. This is shown in Fig. 1, where the simulated energy distributions are compared to their parameterizations for evolution stages $t = 0$ and $t = 6$.

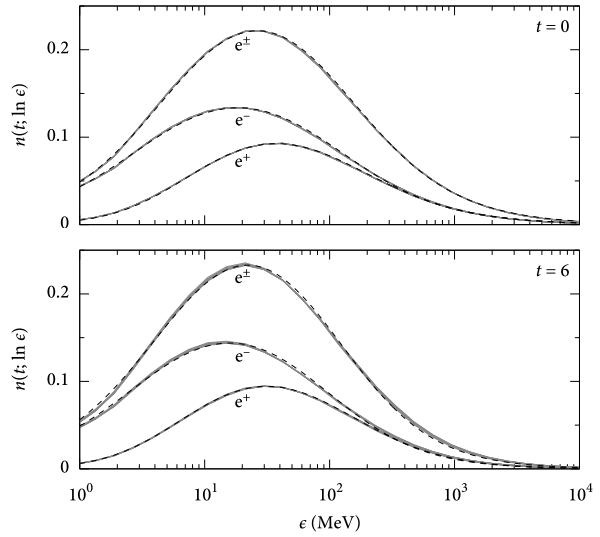

Fig. 1. Average energy distribution for different evolution stages $t = 0$ and $t = 6$ for electrons (marked e^-), positrons (e^+), and their sum ($e^\pm$). Background curves represent simulated distributions for different primaries (p, Fe, and γ) and energies (10^{17}, 10^{18} and 10^{19} eV). The corresponding parameterized distributions from (4) are plotted on top (dashed).

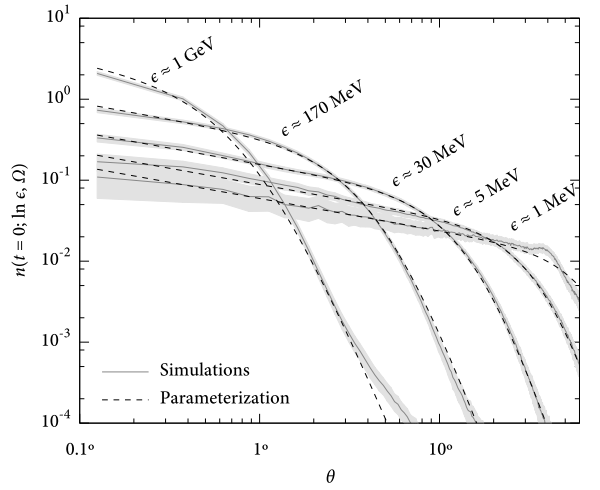

Fig. 2. Normalised average electron distributions $n(t = 0; \ln \epsilon, \Omega)$ (solid) for 20 proton showers at 10^{18} eV with 3σ statistical error margins (filled area). For each energy, corresponding parameterizations according to [8] are also drawn (dashed).

IV. Angular spectrum

The angular distribution of particles is an important factor for observations with Cherenkov and radio telescopes. Fig. 2 shows the average angular distribution of particles at 10^{18} eV as a function of the angle between the shower axis and the particles' direction θ. To compensate for the increase in solid angle with rising θ, the distribution plotted here was divided by $\sin\theta$.

Since the majority of all electrons and positrons stays close to the shower axis, we focus on this part of the distribution. From Fig. 2, it is clear that there is a plateau close to the shower axis at all energies and a sharp drop at a certain angle that depends on secondary energy.

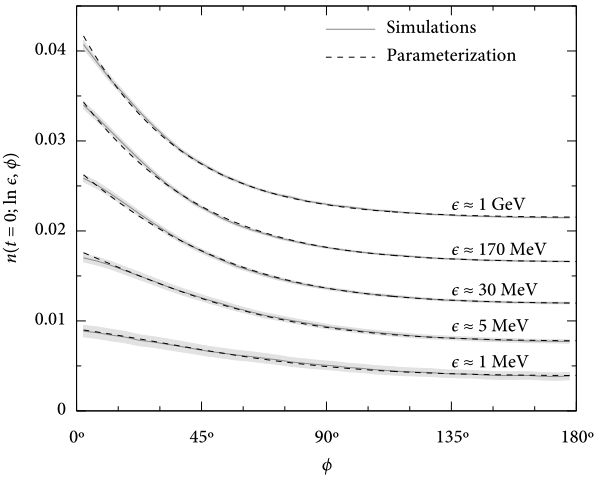

Fig. 3. Normalised average electron distributions $n(t = 0; \ln \epsilon, \phi)$ (solid) for 20 proton showers at 10^{18} eV with 3σ statistical error margins (filled area). Consecutive curves are shifted up by 0.005 to distinguish them better; curves for 1 MeV are at the actual level. For each energy, corresponding parameterizations according to [8] are also drawn (dashed).

Angular distributions were found to be independent of shower stage, as noted earlier [2, 4, 10]. In addition, no dependence on incidence zenith angle or primary energy was found. Looking at different primary species, universality seems somewhat less convincing: spectra for heavier primary species tend to be wider at higher electron energies. The effect is too small to detect, however. The universality with respect to t allows one to parameterize this distribution as a function of two physical quantities only: momentum angle and energy [8].

Because our simulations have no sensitivity in the azimuthal direction by design, no dependence on the geomagnetic field could be determined. Previous work has shown that the effect on the angular distribution is probably small, but not negligible [1, 11]. As accuracy of simulations has rather improved since these studies were carried out, it would be worthwhile to investigate the effect of the geomagnetic field in greater detail.

V. Outward momentum distribution

Let us define ϕ as the angle of a particle momentum vector projected in the plane perpendicular to the shower axis with respect to the outward direction, such that $\phi = 0^\circ$ for a particle moving away from the shower axis, and $\phi = 180^\circ$ for a particle moving towards it. We will refer to this angle as the horizontal momentum angle. For radio measurements, which involve geosynchrotron radiation, this horizontal momentum angle spectrum has to be taken into account [8].

Average simulated distributions $n(t; \ln \epsilon, \phi)$ at $t = 0$ are plotted in Fig. 3 for 20 showers. We observe that high-energy particles tend to move outward more than lower-energy particles. This can be explained by consid-

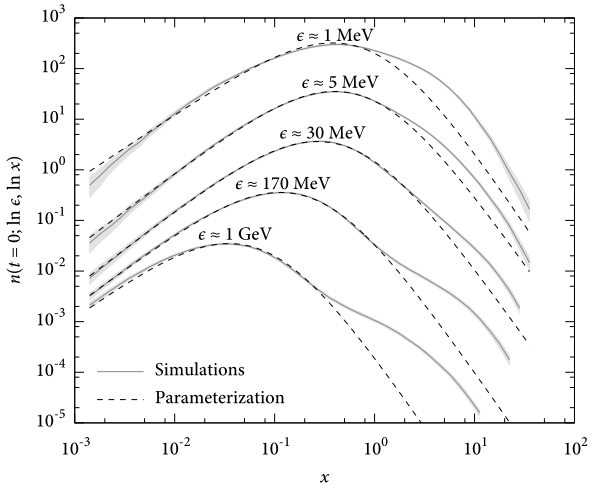

Fig. 4. Normalised average electron distributions $n(t = 0; \ln \epsilon, \ln x)$ (solid) for 20 proton showers at 10^{18} eV with 3σ statistical error margins (filled area). For each energy, corresponding parameterizations according to [8] are also drawn (dashed). Consecutive sets are shifted up by a factor of 10.

ering the collisions in which high-energy electrons and positrons are created, as they primarily occur close to the shower axis. Hence reaction products are transported away from the shower core due to their transverse momenta. Electrons and positrons with lower energies, on the other hand, are also created further away from the shower core.

No significant dependencies on incident zenith angle, primary energy, and primary species were found, so the horizontal momentum angular spectra are universal. Additionally, the shape of the distribution does not change significantly for $\epsilon > 2$ MeV when only electrons or only positrons are considered. There is some dependence in terms of t, however: the distribution appears to soften with evolution stage. This effect can be explained from the expanding spatial structure of the shower with age.

VI. Lateral distribution

When looking at the lateral distribution of electrons and positrons in terms of the lateral distance r from the shower axis, one has to compensate for differences in atmospheric density at the individual values of $X_{\max}$ by expressing the lateral distance in terms of the Molière unit r_{M}, defining $x \equiv r/r_{\mathrm{M}}$ [12].

For different values of ϵ, the normalised average lateral particle distribution at $t = 0$ is shown in Fig. 4 as a function of this quantity. As expected, particles with higher energies tend to remain closer to the shower axis. This agrees with the observation that the angle of their momentum to the shower axis is smaller.

We found no statistically relevant dependence of the lateral distribution on zenith angle of incidence, nor does it change when electrons or positrons are considered separately, except at energies $\epsilon < 10$ MeV. There is, however, a significant effect with shower stage: older showers tend to be wider at the same secondary energy. Therefore, unlike in the case of angular distributions, in any parameterization of the lateral distribution a dependence on t must be incorporated. There is also a minor effect of the energy of the primary on the distribution, but this is only appreciable for secondary energies of $\epsilon > 1$ GeV.

From Fig. 4 it is observed that each curve is a combination of two separate contributions. The left peak, the shape of which does not depend significantly on primary energy or species, is produced through cascading steps of bremsstrahlung and pair creation. The second bulge shows a high level of dependence on primary species, and tends to be less prominent for photon primaries, as for these species there is no significant contribution from the pion production channel. For hadronic primaries it is more significant, especially at higher secondary energies of $\epsilon > 100$ MeV. The magnitude of the variation between different species does not change with t, but its lateral position does slightly.

Theoretically, one could use this difference in lateral distribution to differentiate between primaries on a shower-to-shower basis. But in practice, appreciable difference in density only occurs at high energies and at some distance, implying that the total electron density in the region of sensitivity would be very small. Additionally, the effect does not appear at the same distance for different electron energies, washing out the feature when an integrated energy spectrum is measured.

VII. Delay time distribution

Let us define the delay time Δt of a particle as the time lag with respect to an imaginary particle continuing on the cosmic-ray primary's trajectory with the speed of light in vacuum from the first interaction point. In the distribution of these time lags we must again compensate for differences in Molière radius to obtain a universal description by introducing the variable $\tau \equiv c\Delta t/r_{\mathrm{M}}$, where c is the speed of light in vacuum. The normalised average particle distribution at the shower maximum for different values of ϵ shows a striking resemblance to the time lag distribution to the lateral particle distribution. This similarity is a direct result of the non–planar shape of the shower front as discussed in the next section. Therefore, every characteristic in the lateral distribution will have an equivalent in the time lag distribution. The dependencies on primary energy, species, and angle of incidence closely follow those observed in the lateral distributions in every aspect. This includes the behaviour of the second bulge with primary species. Pion-decay-initiated electrons and positrons are again responsible for the emergence of this peak.

VIII. Shape of the shower front

The similarity between the lateral and delay time distributions of electrons and positrons as investigated in the previous sections is the result of the spatial extent of an air shower at a given time. It makes sense, therefore, to investigate the physical shape of the shower front by

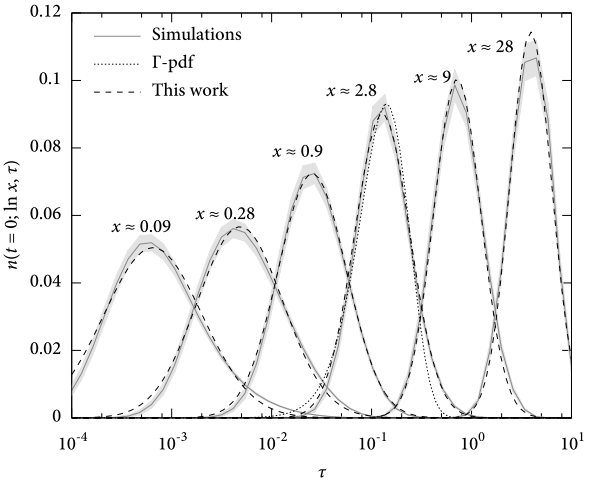

Fig. 5. Average electron distributions $n(t = 0; \ln x, \tau)$ (solid) for 20 proton showers at 10^{18} eV with 3σ statistical error margins (filled area). For each distance, corresponding parameterizations from [8] are drawn as well (dashed). Best-fit Γ-pdfs [13] are also plotted (dotted).

looking at the dependence of the distribution on lateral and delay time simultaneously.

The average shower front shape $n(t; \ln x, \tau)$ for 20 showers at the shower maximum is displayed in Fig. 5 for different distances from the shower core. Though the low number of particles leads to larger fluctuations of the distributions at high distances, the behaviour clearly does not change significantly for $x > 3$.

No significant dependence of the shower front shape on incidence angle or primary energy was found for $x < 15$. There are fluctuations with evolution stage, however: as the shower evolves, the entire distribution shifts to the left. This effect can be explained from the increasing spatial structure of the shower with age, allowing one to estimate $X_{\max}$ from the arrival times of the particles. We also found a non-negligible dependence of the delay time on primary species, which is comparable in nature to the effect of evolution stage. The dependence of the distribution on both species and evolution stage can be removed almost entirely for distances of $0.03 < x < 15$ by applying a simple exponential shift in τ. Additionally, the distributions shown are integrated over energy. Therefore, the shape of the distribution changes when electrons or positrons are considered separately, since their energy distribution is different as well.

The shower front is sometimes approximated as a spherical shell. Close to the shower core, we then expect $\tau \propto x^2$. Going out, the slope should then decrease slowly to a linear relation as x approaches the presumed curvature radius. This spherical shape does not correspond to the situation in our simulations. In the innermost region, we find $\tau \propto x^{1.79}$. Further out, there is an abrupt transition around $x \simeq 0.3$ to $\tau \propto x^{1.45}$.

IX. Conclusion

Analysis of a library of CORSIKA-simulated extensive air showers shows that, to a large extent, their electron–positron distributions show universal behaviour at very high energy, making them dependent on only two parameters: the atmospheric depth $X_{\max}$ and the total number of particles $N_{\max}$ present in the shower at this depth. The entire structure of the shower follows directly from these two values.

Some exceptions to the universality hypothesis were found. Theoretically, these non-universal features can be employed to distinguish primaries on a shower-to-shower basis. In real experiments, however, this would be a difficult task because the effects are very subtle.

X. Acknowledgements

The authors express their gratitude to Markus Risse whose help was indispensable. R.E. acknowledges fruitful discussions with Paolo Lipari on the subject of shower universality. This work is part of the research programme of the 'Stichting voor Fundamenteel Onderzoek der Materie (FOM)', which is financially supported by the 'Nederlandse Organisatie voor Wetenschappelijk Onderzoek (NWO)'. T.H. was supported by grant number VH-NG-413 of the Helmholtz Association.

References

[1] Hillas, A. M. 1982, Journal of Physics G Nuclear Physics, 8, 1461
[2] Giller, M., Kacperczyk, A., Malinowski, J., Tkaczyk, W., & Wieczorek, G. 2005, J. Phys. G, 31, 947
[3] Góra, D., Engel, R., Heck, D., et al. 2006, Astropart. Phys., 24, 484
[4] Nerling, F., Blümer, J., Engel, R., & Risse, M. 2006, Astropart. Phys., 24, 421
[5] Schmidt, F., Ave, M., Cazon, L., & Chou, A. 2008, Astroparticle Physics, 29, 355
[6] Heck, D., Knapp, J., et al. 1998, CORSIKA: A Monte Carlo code to simulate extensive air showers, Tech. Rep. 6019, Forschungszentrum Karlsruhe
[7] Müller. 2008, Diploma Thesis, Univ. Karlsruhe
[8] Lafebre, S., Engel, R., Falcke, H., et al. 2009, Astroparticle Physics, 31, 243
[9] Rossi, B. & Greisen, K. 1941, Reviews of Modern Physics, 13, 240
[10] Giller, M., Stojek, H., & Wieczorek, G. 2005, International Journal of Modern Physics A, 20, 6821
[11] Elbert, J. W., Stanev, T., & Torii, S. 1983, in International Cosmic Ray Conference, Vol. 6, Proc. 18th Int. Cosmic Ray Conf., 227–230
[12] Dova, M. T., Epele, L. N., & Mariazzi, A. G. 2003, Astropart. Phys., 18, 351
[13] Agnetta, G., Ambrosio, M., Aramo, C., et al. 1997, Astroparticle Physics, 6, 301